13B.4

STRUCTURAL CHARACTERISTICS OF TYPHOON SINLAKU (2008) DURING ITS EXTRATROPICAL TRANSITION: AN OBSERVATIONAL STUDY

Julian F. Quinting * and S. C. Jones
Karlsruhe Institute of Technology (KIT), Karlsruhe, Germany

P. A. Harr and M. M. Bell
Naval Postgraduate School (NPS), Monterey

1. INTRODUCTION

Structural changes of a tropical cyclone (TC) during extratropical transition (ET) are responsible for high impact weather in the vicinity of the storm. In addition, the modification of the midlatitude flow by the transitioning TC can even cause high impact weather in regions far away from the ET event. Furthermore, the inaccurate representation of the ET event leads to forecast uncertainties in downstream regions. To understand the physical processes governing these structural changes is a big challenge for meteorologists until today. Because ET events often occur over data-sparse regions previous studies on ET were mainly limited either to model data or to satellite based observations (Klein et al., 2000; Vancas, 2006).

Klein et al. (2000) showed in a seminal study the development of various characteristic structures during the interaction of a TC and the midlatitude baroclinic zone based on infrared satellite imagery. This interaction involves lower tropospheric temperature advection, the deformation of the TC warm core, ascent/descent along the tilted isentropes of the baroclinic zone and lower-tropospheric frontogenesis. In a successive study Harr and Elsberry (2000) showed that the modification of the equivalent potential temperature gradient during ET results in warm frontogenesis in the north eastern quadrant of the transitioning TC. Furthermore, they found that cold frontogenesis to the southwest of the cyclone is often suppressed due to the descent of cold air approaching the TC from upstream regions.

Vancas (2006) utilized temperature retrievals from the Advanced Microwave Sounding Unit (AMSU) to investigate the thermal characteristics of the atmosphere in the vicinity of one ET event. On the base of these retrievals descending cold air to the west and ascending warm air to the east of the transitioning typhoon could be identified.

A first targeted field campaign concerning the ET of TCs was accomplished in 2000 by the Meteorological Service of Canada and the Canadian National Research Council (Abraham et al., 2004).

To extend the knowledge of various physical processes involved in ET on the base of observational data beyond satellite data was a primary goal of the THORPEX-Pacific Asian Regional Campaign (T-PARC) in 2008. During T-PARC one of the major typhoons in the West Pacific in 2008 - Typhoon Sinlaku - was investigated from tropical cyclogenesis until ET in 28 research flights.

Typhoon Sinlaku developed to the east of the Philippines on 8 September and strengthened quickly to typhoon intensity on 9 September. Sinlaku moved northward until 14 September when it recurved on the northern tip of Taiwan. After recurvature the TC moved east-northeastward over the East China Sea and weakened to a tropical storm on 16 September. Instead of decaying soon, the TC re-intensified and re-gained typhoon intensity on 19 September. This re-intensification period was also documented during T-PARC (Sanabia, 2010).

The presented study focuses on Sinlaku's structure on 20 September when the storm approached the midlatitude baroclinic zone and a deep convective system developed.

2. DATASET AND METHODOLOGY

The essential part of this study are airborne observational data that were collected during T-PARC by the NRL-P3 and the USAF-C130 on 20 September 2008. Both aircrafts were equipped with dropsondes and the NRL-P3 additionally with the Electra Doppler Radar ELDORA. For the first time the structure of a transitioning TC was documented simultaneously by two aircrafts. Therefore, the airborne observational data provide unique and detailed insights into a TC approaching the midlatitude baroclinic zone.

To assimilate the various types of measurements (ELDORA, dropsondes, Atmospheric Motion Vectors) into one analysis the recently developed Spline Analysis at Mesoscale Utilizing Radar and Aircraft Instrumentation (SAMURAI) software tool was used. Based on a three-dimensional variational data assimilation approach, this tool offers the opportunity to assimilate observations of various airborne instruments (for details see Bell et al., 2012). The result of this assimilation is the most probable state of the atmosphere for dynamic and thermodynamic variables.

For the presented analysis about 1.7 million observational data, measured between 05 UTC and 08 UTC on 20 September, were assimilated on a domain of 400 *km* $\times$ 400 *km* with a horizontal resolution of 4 *km* $\times$ 4 *km*. The vertical resolution was set to increments of 0.25 *km* up to a height of 15 *km*. As SAMURAI uses the minimization of a cost function by applying a conjugate gradient algo-

* *Corresponding author address:* Julian F. Quinting, Institute for Meteorology and Climate Research (IMK-TRO), Karlsruhe Institute of Technology (KIT), 76128 Karlsruhe, Germany; e-mail: julian.quinting@kit.edu

rithm the operational ECMWF analysis of 20 September, 06 UTC was used as a background estimate.

3. STRUCTURAL CHARACTERISTICS

Using the SAMURAI analysis the small scale structures of Sinlaku and its environment are examined in this section. The data are displayed relative to the best track storm position on 20 September, 06 UTC (Fig. 1, coordinates in km). During the reconnaissance flight the NRL-P3 and the C-130 released in total 30 dropsondes in the analyzed region. The composite of maximum reflectivities shows that the bigger part of ELDORA data was collected to the east and northeast of the best track storm position. The reflectivity composite exhibits maximum values of 42 dBZ. Highest reflectivities concentrate on the southern part of the scanned region (70 km - 110 km E, along 46 km N) and on the northeastern part (200 km E, 160 km N). However, vertical cross sections show that the precipitation structure in the northern part differs completely from that in the southern part of the scanned region.

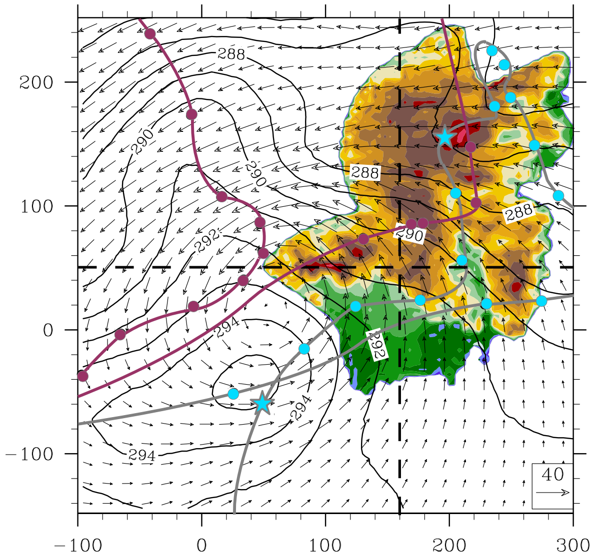

FIG. 1: Maximum reflectivities between 0 km and 15 km [dBZ] (shaded). Colorbar the same as in Fig. 2. Temperature [K] (black contours) and horizontal wind [$m\ s^{-1}$] (vectors) at 1.5 km. Flight track of the NRL P-3 (grey line), flight track of the USAF C-130 (red line). Circles give positions of dropsondes included in the SAMURAI analysis. Dashed black lines show positions of cross sections in Fig. 2.

In a vertical cross section from west to east along 46 km N three cells of deep convection exist (at 100 km E, 170 km E and 250 km E; Fig. 2 (a)). In these convective cells, strong radar reflectivities (24 dBZ) extend up to 8 kilometers and even drop not before 15 km height under 9 dBZ. The absence of a bright band in the radar raw data in this region (not shown) indicates the turbulent structure of the convective cells, which is an important contrast to the precipitation structure in the northern part of the analyzed region. The southern part of the scanned region will be referred to as the deep convective region.

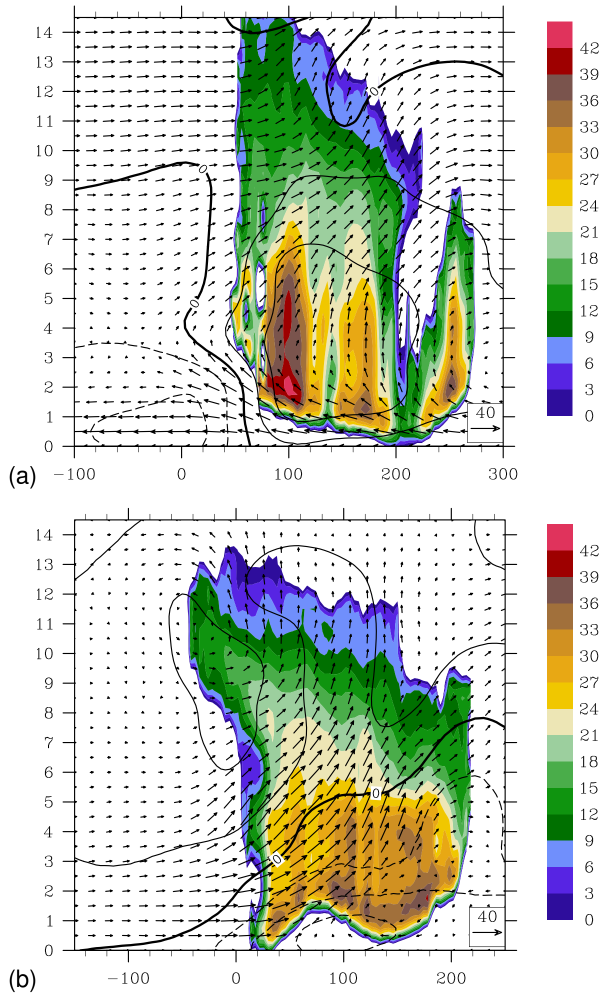

FIG. 2: Reflectivity [dBZ] (shaded) along 46 km N (a) and 160 km E (b). Wind vectors are parallel to cross section [$m\ s^{-1}$]. w is multiplied by ten. Contours denote wind component perpendicular to cross section [$m\ s^{-1}$] (contours with interval of 10 $m\ s^{-1}$). Dashed contours are negative values.

In a vertical cross section from south to north along 160 km E several convective cells can be identified that are similar to those described before (Fig. 2 (b), between 20 km N and 120 km N). But to the north (north of 120 km N), the reflectivity pattern is a lot more homogeneous and somewhat shallower. The radar reflectivity already drops below 24 dBZ at around 6 km height and hence is about 2 km lower than in the deep convective region. The existence of a bright band in the radar raw data (not shown) indicates stratiform precipitation in this region. Fall streaks in the radar raw data enforce this impression. Therefore the northern part of the scanned region will be referred to as the stratiform precipitation region. Due to the chosen SAMURAI configuration with a comparatively coarse vertical and horizontal resolution a bright band and fall streaks can not be identified therein.

From the dual Doppler velocities measured by ELDORA and the dropsonde measurements a three dimensional wind field could be derived. The horizontal wind field exhibits a closed circulation at 1.5 km height (Fig. 1). The center of this closed circulation, i.e. the center of the transitioning TC is located at 10 km N and 50 km E. Strongest winds of about 40 $m\,s^{-1}$ occur to the east and north of the cyclone center. A wind shift from southerly winds in the deep convective region to easterly winds in the stratiform precipitation region produces a confluent zone (50 km N - 120 km N and 60 km E - 180 km E). This confluent region is collocated with a region exhibiting a strong temperature gradient of 4 K within a distance of 70 km. Dropsonde measurements (not shown) as well as the vertical cross section in Fig. 2 (b) show in the same region a vertical wind shift from easterly winds at low levels to southerly winds above. This vertical wind shift of more than 90° indicates strong warm air advection. As a result the examination of the structures illustrated above inevitably leads to the impression of a warm front to the northeast of the cyclone center.

The horizontal wind shifts from northerly to westerly directions to the west-southwest of the circulation center at 1.5 km height (Fig. 1). A strong temperature gradient of 4 K within a distance of 60 km and a counterclockwise rotation of the wind in the vertical from northeasterly winds at low levels to westerly winds above (Fig. 2 (a)) indicate cold-frontal structures.

Another striking feature that needs to be described is located to the south of the circulation center (100 km S - 0 km N and 80 km W- 80 km E; Fig. 1). In this region temperatures exceed 294 K in a westerly flow at 1.5 km. Dropsondes that were released in this region showed a dry layer at this height with a temperature to dewpoint temperature difference of 10 K (not shown). Moreover, the measurements showed an almost dry adiabatic stratification being separated by an inversion of 5 K from a warm moist layer below. This strong inversion associated with an almost dry adiabatic stratification gives the impression of descending airmasses in this region which are interpreted as a dry intrusion.

The vertical cross section in Fig. 2 (a) exhibits a southerly inflow into the system with strongest horizontal winds between 1 km and 6 km height. Westerly winds above 6 km height produce an outflow out of the system at its eastern boundary. The already mentioned southerly inflow into the system in the lower-troposphere ascends into the mid-troposphere in the convective system (Fig. 2 (b)). Two branches of ascent can be distinguished above 5 km. One branch consists of nearly upright ascent between 0 km N and 150 km N. It extends throughout the troposphere and ends in a broad cirrus shield at 14 km height to the south of the deep convection. The second branch ascends slantwise in northerly directions and leaves the analyzed domain between 7 km and 11 km height at 250 km N.

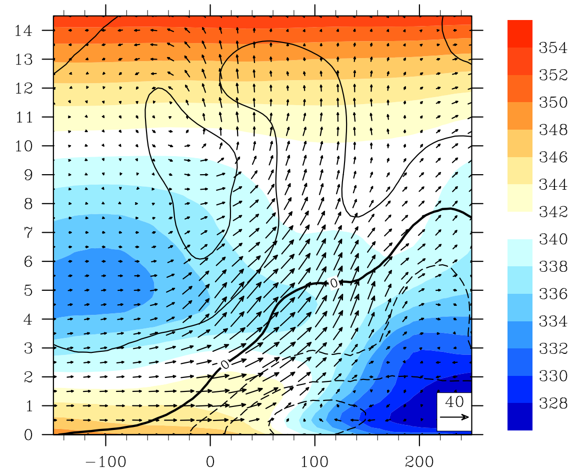

FIG. 3: Moist static energy [$kJ\ kg^{-1}$] (shaded) along 160 km E. Wind vectors are parallel to cross section [$m\ s^{-1}$]. w is multiplied by ten. Contours denote wind component perpendicular to cross section [$m\ s^{-1}$] (contours with interval of 10 $m\ s^{-1}$). Dashed contours are negative values.

To assess the reasons for the convective development the thermodynamic structure needs to be investigated as well. A suitable variable for this investigation is the moist static energy which is a measure of the parcel's kinetic, potential and latent energy. The southern part of the analyzed domain exhibits a potential unstable stratification due to warm moist (tropical) air at lowest levels and cold dry air at mid-levels (Fig. 3). The potential instability is present south of 100 km N but vanishes north of 100 km N. Along 100 km N the stratification is almost neutral due to vertical advection of the low level tropical air within the deep convection and due to slantwise ascent of this low level tropical air along the northward tilted baroclinic zone. Moreover, the slantwise ascent leads to a stable stratification in the stratiform precipitation region with low level cold and dry air. As the deep convection developed in a potential unstable environment a forcing mechanism must have triggered the convective development. A possible trigger mechanism will be discussed in the following section.

4. MECHANISMS

4.1 *Quasigeostrophic forcing*

The role of synoptic-scale forcing on ascent in the warm frontal region and hence in the deep convective region is evaluated by $\mathbf{Q}$ vector diagnostics (Hoskins et al., 1978) derived from the SAMURAI analysis. Applying Hoskins' theory, vertical motion is forced by the divergence of the $\mathbf{Q}$ vector. $\mathbf{Q}$ vector convergence forces ascent and $\mathbf{Q}$ vector divergence forces descent. The interpretation of the $\mathbf{Q}$ vector can be simplified by a natural coordinate partitioning of the $\mathbf{Q}$ vector into a component that is parallel to the isentropes ($\mathbf{Q}_s$) and into a component that is perpendicular to the isentropes ($\mathbf{Q}_n$) (e.g. Martin, 1999). The $\mathbf{Q}_n$ component describes the rate of change of the magnitude of the potential temperature gradient and the $\mathbf{Q}_s$ component describes the rate of change of the direction of the potential temperature gradient.

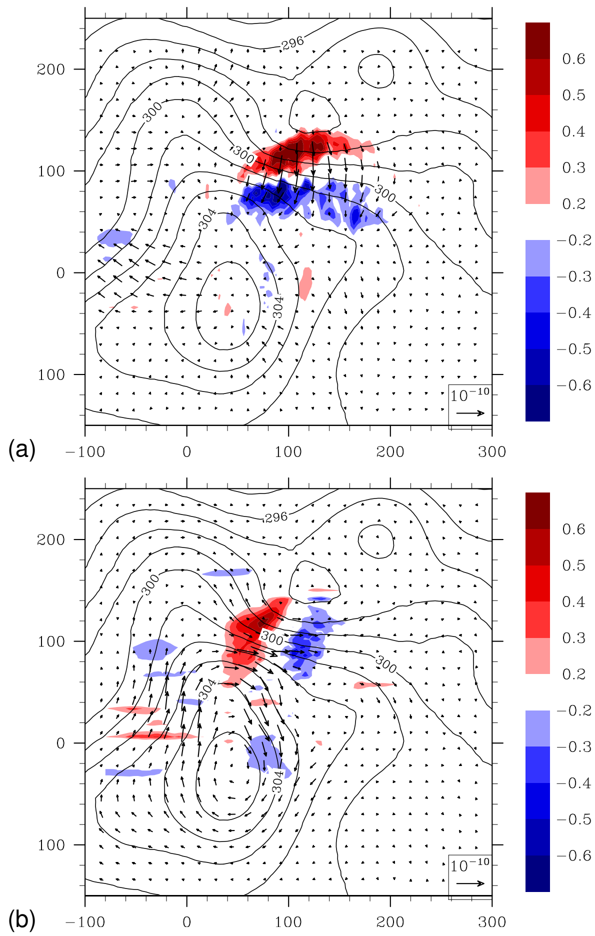

FIG. 4: Vectors and divergence of $\mathbf{Q}_n$ [10^{-14} $m\,(kg \cdot s)^{-1}$] (a) and of $\mathbf{Q}_s$ (b) at 1 km. Contours are potential temperature at 1 km.

Banded regions of $\mathbf{Q}_n$ divergence and convergence exist in the region of strongest baroclinicity at 1 km height (Fig. 4 (a)). $\mathbf{Q}_n$ convergence is located in the southern part of the baroclinic zone whereas $\mathbf{Q}_n$ divergence is located in the northern part of the baroclinic zone. This quasi-dipole structure of $\mathbf{Q}_n$ is maintained up to 3.5 km height. The maximum of $\mathbf{Q}_n$ convergence is collocated with the deep convective region (40 km N - 80 km N and 60 km E - 120 km E). This collocation indicates that $\mathbf{Q}_n$ convergence due to frontogenetic processes presumably triggered the deep convective development in a potential unstable environment.
The influence of the cyclonic wind field on the temperature field can be assessed by evaluating $\mathbf{Q}_s$. Strongest $\mathbf{Q}_s$ divergence occurs in the region of a thermal trough to the north of the cyclone (Fig. 4 (b)). To the east of this region covergence of $\mathbf{Q}_s$ can be found. The observed dipole pattern with adjacency of $\mathbf{Q}_s$ convergence and divergence indicates an amplification of the thermal wave with a deepening thermal trough and a strengthening thermal ridge. However, the magnitude of $\mathbf{Q}_n$ divergence/convergence is stronger than the magnitude of $\mathbf{Q}_s$ divergence/convergence so that $\mathbf{Q}_n$ has a stronger impact on vertical motion and on the temperature field. Although this investigation of $\mathbf{Q}_n$ and $\mathbf{Q}_s$ is typical of an intensifying midlatitude cyclone, Sinlaku did not reintensify in the following days according to the ECMWF analysis (not shown).

4.2 *Potential vorticity*

In a final step the influence of the deep convection on the cyclone needs to be investigated. Therefore, the potential vorticity (PV) structure derived from the SAMURAI analysis is analyzed. A strong positive PV anomaly characterizes the low level PV structure and is collocated with Sinlaku's circulation center (Fig. 5 (a)). This low level PV anomaly decreases with height and reaches its minimum at 3 km (not shown). A restrengthening of the PV can be noticed above 3 km height in the deep convective region. This results in a second PV maximum at 6 km height with PV values of more than 5 Potential Vorticity Units (PVU) (Fig. 5 (b)). This maximum is in the region of the highest reflectivity values and thus associated with the deep convection. A consideration of the observed structures leads to the conclusion that the PV-maximum at mid-levels is a result of latent heat release due to steady condensation within the deep convection. A closed circulation around Sinlaku does not exist at 6 km. The wind field exhibits a circulation that is elongated from south to north with its apex close to the PV maximum. Therefore we assume that Sinlaku's wind field was modified by latent heat release, respectively PV production in the region of the deep convection. Another region of enhanced PV of more than 4 PVU can be identified at 6 km in the stratiform region (120 km E - 200 km E and 140 km N - 220 km N; Fig. 5 (b)). Vertical cross sections through this region exhibit a PV tower up to 11 km height (not shown). This PV tower results from steady condensation in the stratiform precipitation region along the frontal zone. This PV tower is lifted about 2 km from the surface in the region of the baroclinic zone. Its elevation from the surface is a result of evaporation at lowest levels that leads to a reduction of PV.

5. SUMMARY AND OUTLOOK

This study investigates the structure of Typhoon Sinlaku (2008) during ET on the base of airborne observational data from T-PARC. By assimilating ELDORA data as well as dropsonde data with the recently developed software tool SAMURAI, a highly resolved analysis of the dynamic and thermodynamic features could be derived. Most of the ELDORA data were collected to the north and east of the cyclone center in a convective system that developed

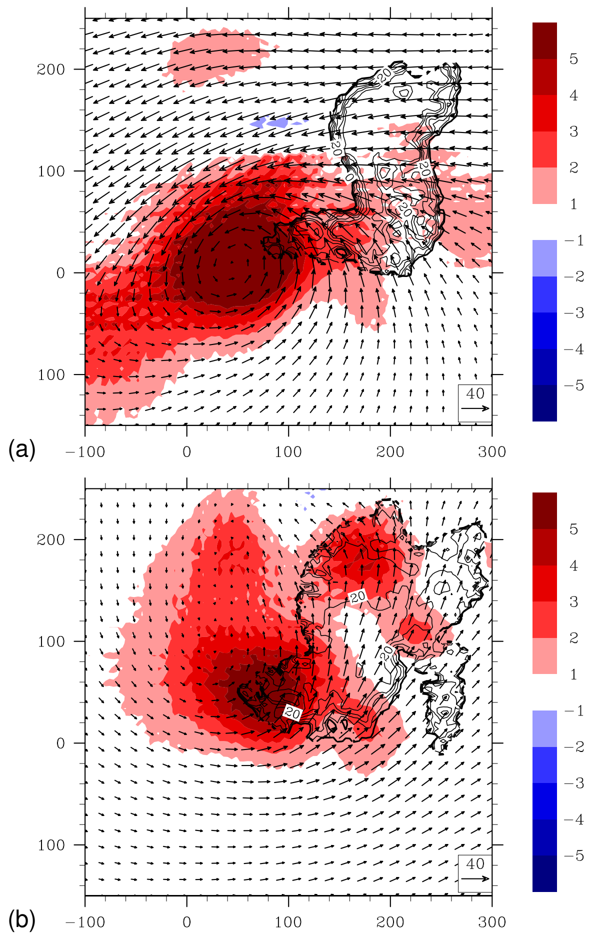

FIG. 5: Potential vorticity [PVU] (shaded) and reflectivity [dBZ] (contours) at 1 km (a) and 6 km (b) derived from the SAMURAI analysis. Vectors give horizontal wind.

as Sinlaku approached the midlatitude baroclinic zone. Dropsonde measurements were accomplished around the cyclone by the USAF-C130 and the NRL-P3. Based on the obtained analysis we were able to identify a deep convective region, a stratiform precipitation region, warm and cold frontal structures and a dry intrusion in the vicinity of the transitioning TC. The convective system developed on the warm frontal zone. It is determined by almost upright upward motion and ascent along the moist isentropes of the northward tilted midlatitude baroclinic zone. The investigation of the moist static energy showed that the convection developed in a potential unstable environment.

$\mathbf{Q}$ vector diagnostics suggest that forced ascent triggered the deep convection in this unstable environment. Furthermore, the partitioning of the $\mathbf{Q}$ vector indicated an amplitudinal growth of the thermal wave initiated by Sinlaku's circulation.

An investigation of the PV structure showed a maximum of PV at mid-levels being collocated with the center of the deep convection. This indicates the production of PV by latent heat release in the convective region. The strong production of PV led to a deformation of Sinlaku's wind field and hence influenced presumably the TC's decay.

In future studies it would be a challenging task to perform simulations with a high spatial resolution which are able to represent the main observed structures. To confirm the identified mechanisms and investigate the sensitivity of simulations towards these mechanisms would be a further challenging topic.

Acknowledgments

We would like to acknowledge the Helmholtz ATMO Programm for supporting T-PARC research flights and for enabling Julian Quinting to visit the Naval Postgraduate School, Monterey. This work was conducted as part of the research unit PANDOWAE (FOR896), funded by the German Research Council (DFG). We would like to thank the ECMWF for providing analysis data under the special project spdeet.

REFERENCES

Abraham, J., J. Strapp, C. Fogarty, and M. Wolde, 2004: Extratropical transition of Hurricane Michael: An aircraft investigation. *Bull. Amer. Meteor. Soc.*, **85**, 1323–1339.

Bell, M. M., M. T. Montgomery, and K. E. Emanuel, 2012: Air-sea enthalpy and momentum exchange at major hurricane wind speeds observed during CBLAST. *J. Atmos. Sci.* submitted.

Harr, P. and R. Elsberry, 2000: Extratropical transition of tropical cyclones over the western North Pacific. Part I: Evolution of structural characteristics during the transition process. *Mon. Wea. Rev.*, **128**, 2613–2633.

Hoskins, B. J., I. Draghici, and H. C. Davies, 1978: A new look at the ω-equation. *Quart. J. Roy. Meteor. Soc.*, **104**, 31–38.

Klein, P., P. Harr, and R. Elsberry, 2000: Extratropical transition of western North Pacific tropical cyclones: An overview and conceptual model of the transformation stage. *Wea. Forecasting*, **15**, 373–395.

Martin, J., 1999: Quasigeostrophic Forcing of Ascent in the Occluded Sector of Cyclones and the Trowal Airstream. *Mon. Wea. Rev.*, **127**, 70–88.

Sanabia, E. R., 2010: The re-intensification of Typhoon Sinlaku (2008). Master's thesis, Naval Postgraduate School, Monterey, 213. [Available online at http://handle.dtic.mil/100.2/ADA524716].

Vancas, M., 2006: The Extratropical Transition of Tropical Storm Banyan. Master's thesis, Naval Postgraduate School, Monterey, 90. [Available online at http://edocs.nps.edu/npspubs/scholarly/theses/2006/Sep/06Sep_Vancas.pdf].